MEASUREMENTS AND CALCULATIONS OF GATE RUDDER PERFORMANCE

Noriyuki Sasaki, Newcastle University, UK.
Sadatomo Kuribayashi, Kuribayashi Steam Co. Ltd., Japan
Nobuhiro Asaumi Yamanaka Shipbuilding Co. Ltd., Japan
Masahiko Fukazawa, Kamome Propeller Co. Ltd., Japan
Takao Nonaka, Tokyo Keiki Co. Ltd., Japan
Serkan Turkmen, Newcastle University, Japan
Mehmet Atlar, University of Strathclyde, UK

Rudder is one of the most important elements of a ship system by which the horizontal ship motion can be controlled effectively to keep the desired track in navigation. Rudder is usually placed behind a propeller to create effective steering forces by using the propeller's slipstream. It is also a well-known fact that the rudder induces an additional drag which is an undesirable source for performance loss of a ship.

A new concept rudder system, which is called "Gate Rudder", has been introduced recently by a system of twin rudder blades where each blade is located aside a propeller rather than behind the propeller. Each of the twin blades can be controlled independently for effective thrust vectoring whilst the asymmetric and cambered sections of the blades generates additional thrust acting as the duct of an accelerating ducted propeller system. This energy efficient and superior maneuvering control system was originally invented by Kuribayashi in 2012 and has been developed further by the past and ongoing collaborative R&D activities including a wide range of model tests and computational works.

In this paper, we are presenting a recently developed dedicated design analysis and simulation software to predict the performance of a gate rudder system. The software has been developed as a practical design tool by which one can analyse and simulate the performance of a ship equipped with a gate rudder system accurately by taking into account the interaction between the asymmetric rudder blades and the propeller effectively.

Nomenclature

A_P	Propeller disc area (m^2)	L_{ij}^{mn}	Influence coefficient	α_E	Effective attack angle (rad)
A_R	Rudder are (m^2)	$\vec{n}$	Normal vector	α_G	Geom. attack angle (rad)
$c(y)$	Chord length (m)	p	Propeller pitch (m)	α_0	Zero-lift angle (rad)
$C_D(y)$	Drag coefficient	Q	Torque (N-m)	λ	Aspect ratio
$C_L(y)$	Lift coefficient	r	Propeller radius (m)	θ	Blade angle (rad)
C_Di	Induced drag coefficient	r_M	Blade strip radius (m)	ρ	Fluid density (kg/m^3)
C_F	Frictional drag coefficient	T	Propeller thrust (N)	ψ	Flow angle (deg.)
C_T	Prop loading coefficient	$t(y)$	Blade thickness (m)	Γ_{ij}	Circulation (N m^2/Kg/sec)
$D(y)$	Drag per length (N/m)	V^*	Total velocity (m/sec)		
f	Immergence of Prop. (m)	U	Axial velocity (m/sec)		
F_N	Normal Force (N or Kgf)	V	Vertical velocity (m/sec)		
h	Prop. hydrodynamic pitch	W	Horizontal velocity (m/sec)		
K_{ij}^{mn}	Influence coefficient	V_0	Prop. Advance speed (m/sec)		
$L(y)$	Lift per length (N/m)	V_S	Ship speed (m/sec)		

1. Introduction

Hydrodynamic mechanisms for the propulsive energy saving of a ship can be based on:

(1) Recovery of propeller rotational losses by fins which are placed in front of or after a propeller (e.g., pre- or post-swirl devices);

(2) Recovery of viscous resistance losses by ducts or fins which are placed in front of a propeller to generate thrust in addition to the propeller thrust.

Within the above framework, newly introduced *"Gate Rudder"* concept is also an energy saving system for ships but its saving principle is somehow different from the present saving systems in terms of its location and functioning. The conventional energy saving devices are located in front of a propeller or behind, and ship's rudder can also serve as a base where the energy saving device can be attached to. There are many energy saving devices which are installed on the leading edge of ship's rudder and just behind the center of the propeller where the density of the energy loss due to the propeller action is the highest.

In a Gate Rudder system, two asymmetric rudder blades are located aside the propeller by shifting the classical single rudder blade from the slipstream of the propeller. By this arrangement the two rudder blades do not only act as rudder but also function, partially, as the duct of an accelerating ducted propeller system. This means the rudder blades generate thrust, like an accelerating duct, as opposed to creating resistance by the conventional rudder system.

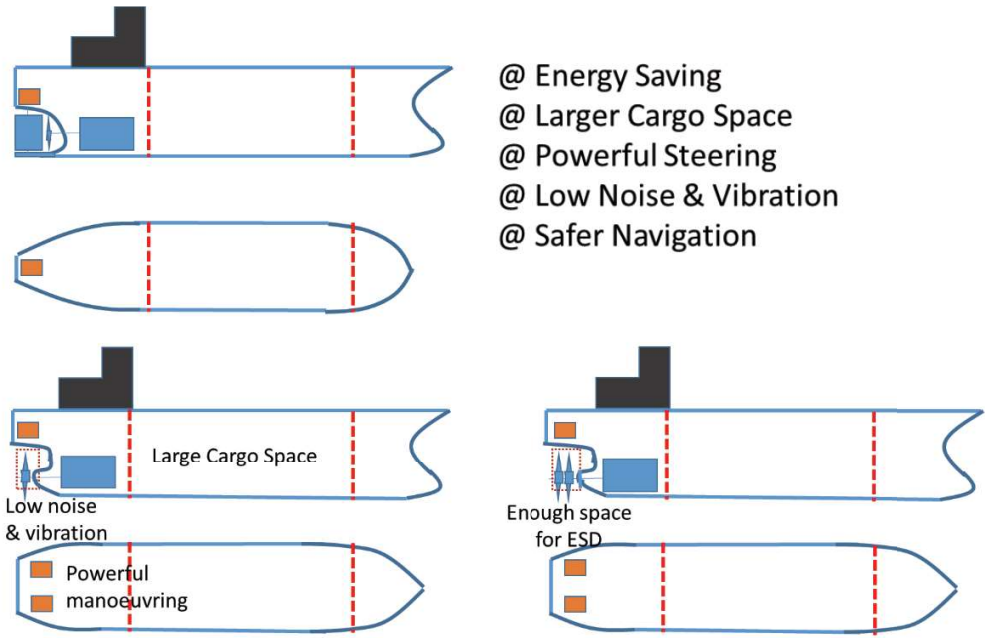

Fig. 1 Future stern shapes obtained from Gate Rudder Application

The application of a gate rudder system, schematically summarized in Figure 1, can brought about the potential overall benefits for a ship which can be grouped in the following three main areas[6]:

- Economical-

(1) Higher propulsive efficiency owing to the duct effect of the gate rudder
(2) No torque rich or improved torque rich condition for engine provided by manual or active control of the gate rudder helm angles
(3) Larger cargo space by shifting the engine room afterward due to space saving of the conventional rudder removed from the propeller's slipstream for a fixed ship length
(4) Shorter ship length by replacing conventional rudder with a gate rudder system

- Safety-

(5) Remarkable maneuverability by independently controlled twin rudder blades of the gate rudder system
(6) Remarkable stopping ability
(7) Remarkable berthing performance (with efficient crabbing maneuver)
(8) Improved rolling motion of a ship by independent controlled gate rudder blade angles

- Habitability-

(9) Reduced propeller induced underwater radiated noise (URN) and vibrations due to the equalized stern (wake) flow created by the gate rudder system
(10) Larger accommodation space by shifting engine room further afterwards with the gate rudder system

Whilst the above benefits are associated with the gate rudder system, the exploitation of these benefits requires accurate modeling of the hydrodynamic interaction between the rudder blades of a gate rudder with it is propeller which is similar to the interaction between the duct and impeller of an accelerating duct. This is turn would require the development of dedicated computer programs which need to be validated and verified by model tests.

This paper introduces the development of such simulation methodologies, their applications and comparison of the predictions with the model tests conducted at several model testing facilities.

2. Theoretical approaches for predictions of rudder blade forces and flow field of a gate rudder system

2.1. Blade element theory with 3D correction

According to the blade element theory, the formulation for a gate rudder thrust (T_{GR}) is based on a following equation;

$$T_{GR} = \int_{btm}^{top} L(y)\cos\psi(z) - D(y)\sin\psi(y)dz - R_{SFT} \tag{1}$$

where, R_{SFT} represents the resistance of the rudder shafts which are exposed in the stern flow and this is relatively large compared with conventional rudder because the velocity at gate rudder shafts is higher than those of conventional rudder.

In equation (1), lift $L(y)$and drag $D(y)$ are formulated in by using;

$$\begin{aligned} L(y) &= \frac{1}{2}\rho V^{*2} * C_L(y) * c(y) \\ D(y) &= \frac{1}{2}\rho V^{*2} * C_D(y) * c(y) \\ V^* &= \sqrt{V_x^{\,2} + V_z^{\,2}} \\ \psi &= \tan^{-1}(\frac{V_z}{V_x}) \end{aligned} \tag{2}$$

where, vertical distribution of lift coefficient $C_L(y)$ and drag coefficient $C_D(y)$ can be calculated by following equations if we can use a co-ordinate system shown in Fig.2;

$$\begin{aligned} C_L(y) &= 2\pi \sin(\psi - \alpha_0)\frac{\lambda}{2.3+\lambda} \\ C_D(y) &= 2 * C_F * (1 + \frac{t(y)}{c(y)})) + (\frac{t(y)}{C(y)})^2 + C_{Di} \\ C_{Di} &= \frac{C_L^{\,2}}{\pi\lambda} \end{aligned} \tag{3}$$

The theory is very simple and predictions can be robust as far as the predicted values are validated and supported by many experimental data. However, as one may note, the method can only be used if the appropriate flow velocities and angles of attack are known. This means we have to use other prediction tools to estimate the flow velocities and angles of attack at each section by properly taking the interaction between the propeller and rudders.

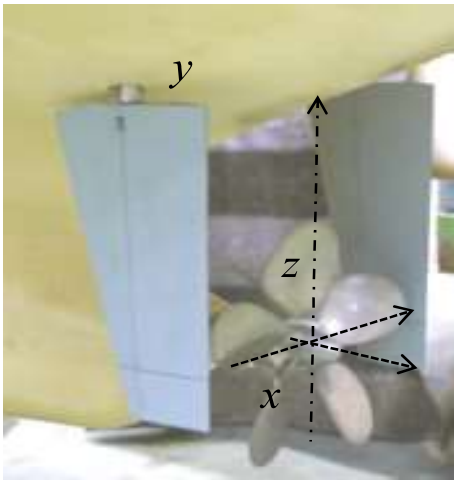

Fig.2 - Co-ordinate system of Rudders & Propeller

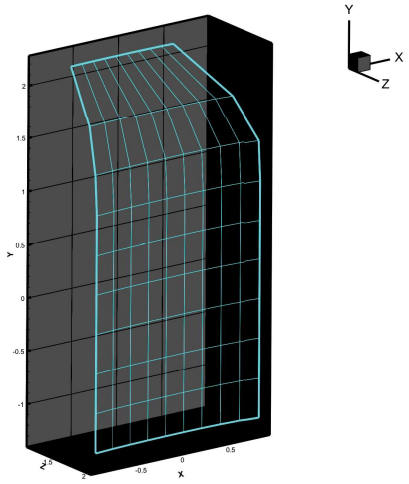

Fig.3 - Grid Generation of Gate Rudder

In order to tackle the above described flow velocity and angle of attack prediction problem, in this paper, four different theoretical modelling were used in combination: these involved an axial momentum theory based modelling; a lifting surface theory, a linearized vortex lattice based modelling and a commercial CFD code.

Because the rudder blades are located in the vicinity of the propeller plane, the propeller induced velocities should be estimated with reasonable accuracy. According to the axial momentum theory, the flow velocities behind a propeller can be formulated as in Equation (4);

$$V_X = V_0 * \varepsilon \cdot (1 + C_T)^{0.5} \tag{4}$$

where V_O is propeller advanced speed which can be measured during the self propulsion test and calculated by Equation (5) using the effective wake w_T;

$$V_0 = V_S \cdot (1 - w_T) \tag{5}$$

In Equation (4) C_T is the propeller loading coefficient and defined by

$$C_T = \frac{T}{0.5\rho V_O{}^2 A_P} \tag{6}$$

where, T is propeller thrust, A_P is disk area of the propeller, ε is a function of x/D_P and r/R and its value can be fixed around 0.7-0.9 depending the geometry and configuration of the propeller and rudder.

Although the theory can only predict the axial volume mean velocity inside the propeller slip stream, it will be still useful for the prediction of the flow field of the gate rudder since the theory can predict the outer radii regions of the propeller slip stream reasonably accuarate and this can be a close prediction of the gate rudder flow field.

2.2. Linearized Vortex Lattice Method (VLM)

The linearized vortex lattice method (VLM) was used for the prediction of rudder performance and it was implemented into an iterative calculation procedure which will be explained later. According to the VLM, the rudder surface is divided into number of panels which have M*N rows and columns as shown in Figure 3. The elementary force acting on the X and Z direction of the rudder are given in Equation (7)

$$F_X = \sum_{i=1}^{M}\sum_{j=1}^{N} L_{ij} \cdot \sin \alpha_{g\,ij}$$
$$F_Z = \sum_{i=1}^{M}\sum_{j-1}^{N} L_{ij} \cdot \cos\alpha_{g\,ij} \tag{7}$$

Where

$$L_{ij} = \rho \cdot U^* \cdot \cos(\alpha_e - \alpha_g ij) \cdot \Gamma_{ij} \cdot S_{ij} \tag{8}$$

$$U^* = (U_X{}^2 + U_Z{}^2)^{0.5}$$
$$\alpha_e = \frac{U_Z}{U_X} \tag{9}$$
$$\alpha_g ij = (\frac{\partial Z}{\partial x})ij$$

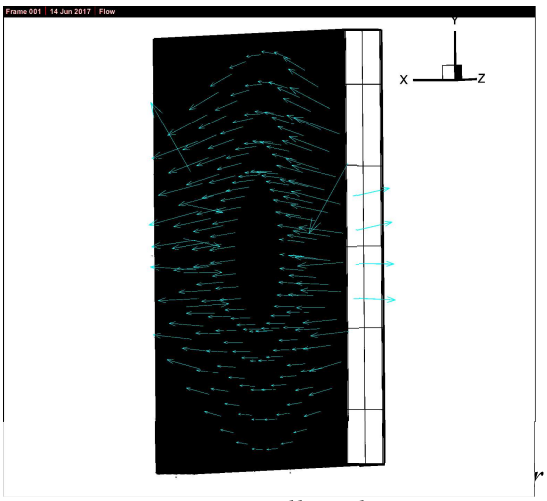

in a Propeller Plane

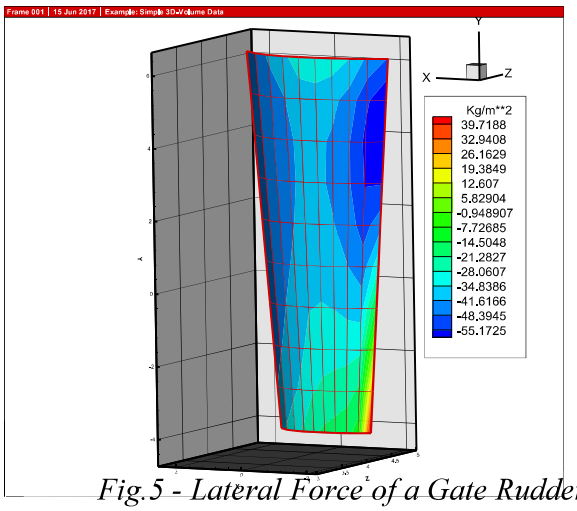

Fig.5 - Lateral Force of a Gate Rudder due to propeller action

U, W is the velocity component in X and Z direction at infinity upstream, respectively, and α_g(i,j) is the tangent of wing surface at the control point of panel (i , j).

In Equation (8) the circulation of panel (i , j) with strength Γ_{ij}^{mn} can be obtained by solving the linear equation system given in Equation (10)

$$\sum_{m=1}^{M} \cdot \sum_{n=1}^{N} \Gamma_{mn} \cdot K_{ij}^{mn} = U_X(\alpha_g ij - \alpha_e) \tag{10}$$

where K_{ij}^{mn} is the influence coefficient between panel (i , j) and a vortex filament (m , n) with strength Γ_{mn}. Equation (11) can be used to predict induced velocity W_U from vortex filament (m , n) at the control point of panel (i , j).

$$W_U = K_{ij}^{mn} \cdot \Gamma_{mn} \tag{11}$$

The body boundary condition of the wing surface is given in Equation (12) assuming that the disturbance velocity is small in comparison with free stream velocity;

$$(\vec{U} + \sum \vec{W}_U) \cdot \vec{n} = 0 \tag{12}$$

Having described the vortex lattice model of the rudder surfaces next will be the description of the propeller flow model based on a simple lifting surface theory.

2.3. Simple Propeller Theory

The simple propeller theory developed by Yamasaki [7] was used for the propeller flow modelling in this study except some parts where a CFD method with the body force approach is preferred.

The Yamasaki model is more complicated than the body force model of CFD and it was introduced for the sake of solving the interaction problem between a propeller and a rudder (s) which is the most critical aspect in accurate prediction of the gate rudder performance.

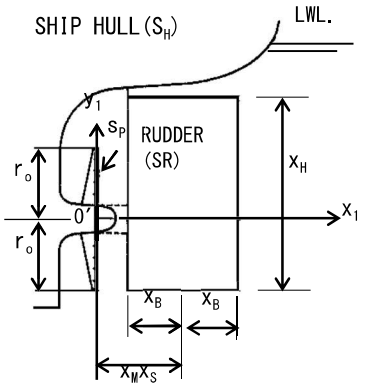

Fig.6 - Co-ordinate system of Rudder & Propeller [8]

In this theory, the circulations with strength Γ_{mn} are distributed on the propeller plane which is divided into $\overline{M} \times \overline{N}$ panels. The flow around the propeller can be obtained from the induced velocities of two vortex systems, one is bound vortex and other is free vortex shedding from the bound vortex. The strength of circulation Γ_{mn} is obtained by solving governing equations based on the boundary conditions on the propeller blade surfaces.

By using the circulations and influence coefficients derived from Biot-Savart equation, the flow velocities at the rudder position can be obtained as follows:

In -X direction, velocity component Vx becomes as:

$$V_X = \frac{1}{4\pi} \sum_{m=1}^{\overline{M}} \sum_{n=1}^{\overline{N}} V\Gamma_{mn}(P_X) \tag{13}$$

where、

$$\begin{aligned}
&(P_X) = P_x(rm, \theta n)\Delta r \Delta\theta, \\
&P_X(r', \theta') = \{-r'x_1/h - y\sin\theta' + \cos\theta' \}/R_3^3 \\
&+ \{-r'x_1/h - (2f - y)\sin\theta' + z\cos\theta' \}/R_4^3, \\
&R_3^2 = x_1^2 + r'^2 - 2r'(y\cos\theta' + z\sin\theta') + y^2 + z^2, \\
&R_4^2 = x_1^2 + r'^2 - 2r'\{(2f - y)\cos\theta' + z\sin\theta' \} + (2f - y)^2 + z^2
\end{aligned} \tag{14}$$

In -Z direction at the rudder centre velocity component $(W_P)_{(SR)}$

$$(W_p)_{(SR)} = \frac{V}{4\pi}\sum_{\substack{m=1\\ m\neq}}^{\bar{M}}\sum_{\substack{n=1\\ h-7}}^{\bar{N}}\Gamma_{mn}P_z(x_{1,}y_h,o;r'_{m,}\theta'_n)\Delta r\Delta\theta$$

$$+\frac{V}{4\pi}\sum_{n=1}^{\bar{N}}(\Gamma_{mn}-\bar{\Gamma}_{m1})P_Z(x_{1,}r_{m,}o;r'_{\mathrm{m}},\theta'_n)\Delta r\Delta\theta, for \quad y_\kappa > 0 \tag{15}$$

$$(W_p)_{(SR)} = \frac{V}{4\pi}\sum_{\substack{m=1\\ m\neq}}^{\bar{M}}\sum_{\substack{n=1\\ h-6}}^{\bar{N}}\Gamma_{mn}P_z(x_{1,}y_h o;r'_{m,}\theta'_n)\Delta r\Delta\theta$$

$$+\frac{V}{4\pi}\sum_{n=1}^{\bar{N}}(\Gamma_{mn}-\bar{\Gamma}_{m2})P_Z(x_{1,}r_{m,}o;r,\theta_n)\Delta r\Delta\theta, for \quad y_\kappa < 0$$

where

$$\begin{aligned}
&\bar{\Gamma}_{m1}\left(\Gamma_{m1}+\Gamma_{m36}\right)/2\\
&\overline{\Gamma_{m2}} = (\Gamma_{m18}+\Gamma_{m19})/2\\
&\mathrm{P}_z(x_{1,}y,o;r'\theta') = \frac{r'^2\cos\theta' - 2r'y + y^2\cos\theta'}{A_1^2}(1+\frac{x_1}{\sqrt{x_1^2+A_1}})\\
&+(\frac{r'}{h}+\frac{-x_1 y\sin\theta'}{A_1})\frac{r'\sin\theta'}{(x_1^2+A_1)^{3/2}}+\\
&\frac{r'^2\cos\theta' - 2r'(2f-y)+(2f-y)^2\cos\theta'}{B_1^2}(1+\frac{x_1}{\sqrt{x_1^2+B_1}})\\
&+(\frac{r'}{h}+\frac{-x_1(2f-y)\sin\theta'}{B_1})\frac{r'\sin\theta'}{(x_1^2+B_1)^{3/2}}\\
&A_1 = r'^2 - 2r'y\cos\theta' + y^2,\\
&B_1 = r'^2 - 2r'(2f-y)\cos\theta' + (2f-y)^2
\end{aligned} \tag{16}$$

The comparion of the induced velocities calculated by the Axial Momentum Theory and Simple Propeller Theory is shown in Figure 7 (left) where $\varepsilon = 0.85$ was used for the momentum thoery. As opposed to the earlier described Axial Momenttum theory, the Simple Propeller Theory can model the propeller slip stream within more details and accurate as shown in Figure 7 (right) while the axial momentum theory can only predict the mean value (red line of Fig.7) on the propeller plane.

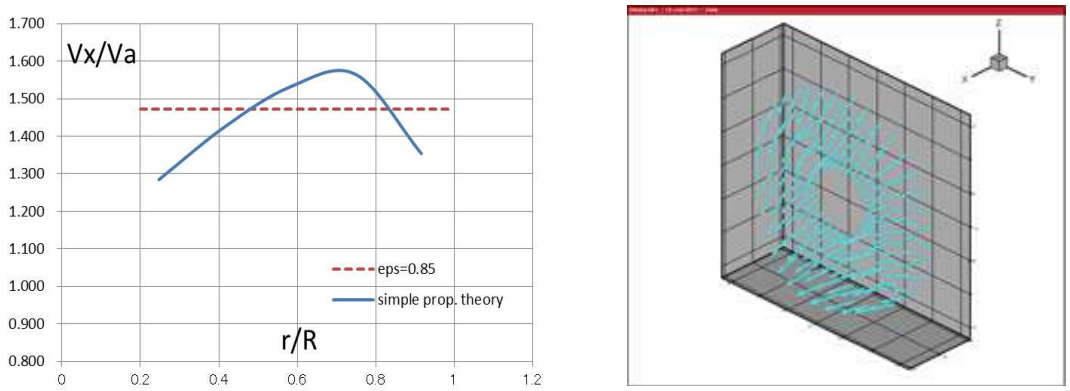

Figure 7 - Propeller slip stream obtained by axial momentum theory and Simple Propeller Theory

2.4. Computational Fluid Dynamics (CFD) method

The key issue to determine the rudder force of the gate rudder is how large are the parts exposed in the propeller race. To overcome this issue the computation by Computational Fluid Dynamics (CFD) based on the Navier-Stokes equation solver was employed. The CFD calculation can predict even strong vorticities and separation phenomena which may occur in the stern flow. The data of flow fields obtained from CFD calculations was used in order to provide the input data for the other theories introduce in Section 2.

Commercial CFD package Starccm+ finite volume stress solver was employed for the prediction of flow field around the gate rudder for not only straight forward condition but also yaw conditions (oblique conditions). The flow fields depend on the propeller rotation direction as well as the rudder angle. The propeller performance characteristics were also introduced in the CFD model as a momentum source to simulate the propeller action. , k-ω Shear Stress Transport (SST) was chosen for the effect of turbulence on the single flow domain (water).
Fig.7 shows a grid generation for the calculation of flow fields around the gate rudder. Refinement was applied around the propeller disc and near field to the hull.

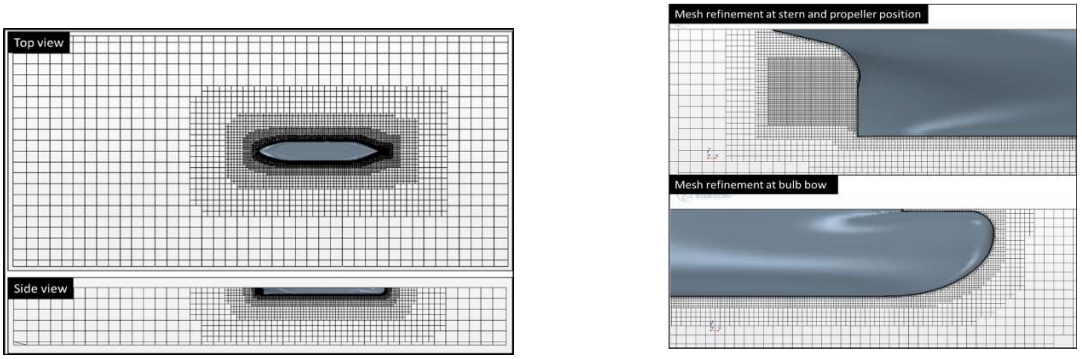

Fig.7 grid generation for container ship with gate rudder

Fig. 8 presents the results of calculation are shown on a virtual cylindrical plane. The virtual cylinder is a wake and used to predict velocities around the gate rudders to estimate the flow induced forces generated by gate rudder. A sketch is added in top right of Fig 8 to demonstrate the cylinder.

The cylindrical plane (wake) represents the surface in which the centre of the gate rudder is moving when it is steered. β is yaw angle in degree of the ship. On the cylindrical plane, the propeller slip stream can be clearly seen and the effect of yaw angles appears on the non-symmetrical shape of propeller slip stream.

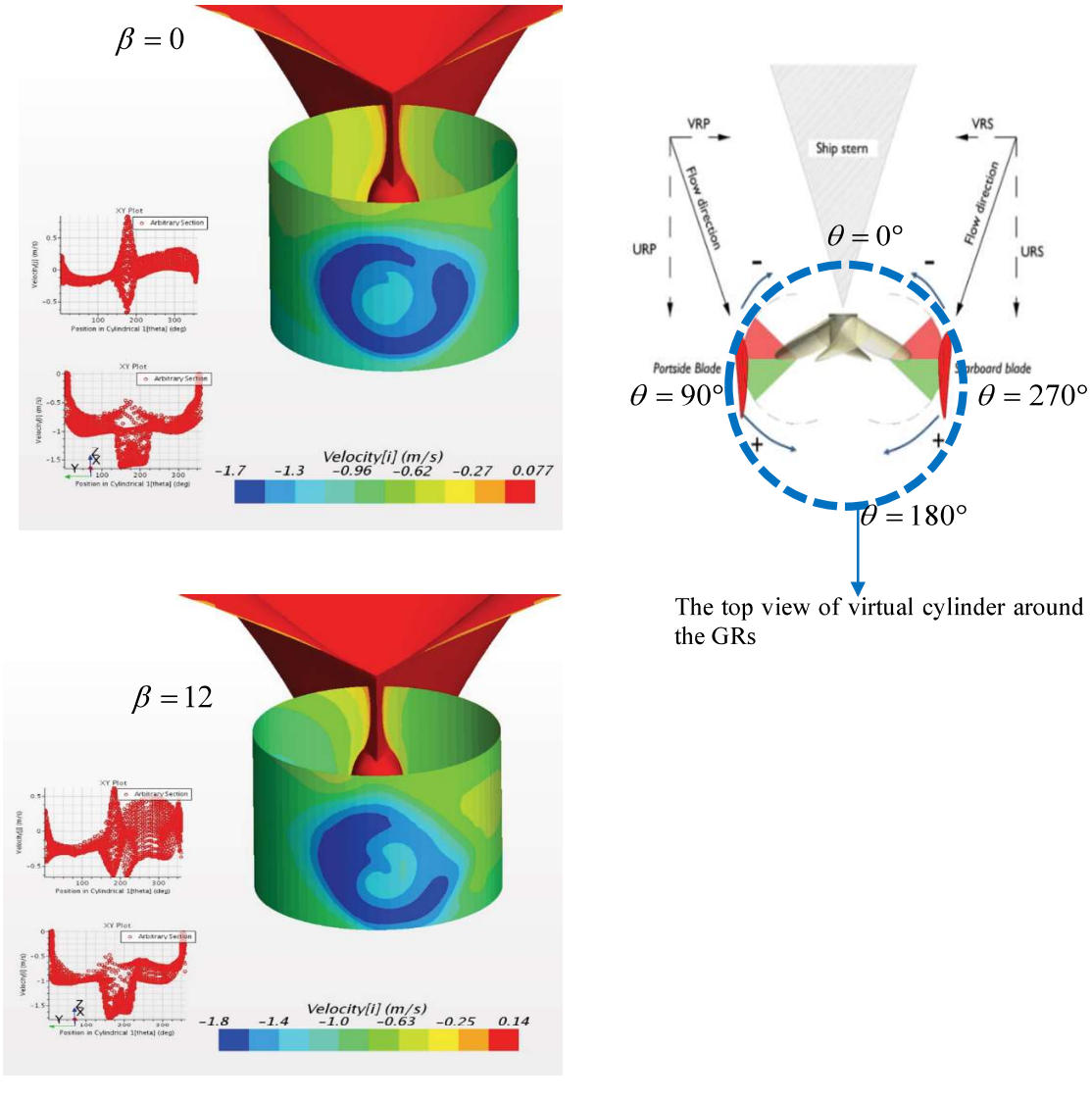

Fig. 8.Velocity field of container ship obtained by CFD

Error! Reference source not found.8 (top) shows the axial velocity without yaw angle condition on the surface of circular cylinder with radius *Sb*. *Sb* means distance between ship center line and rudder blade at zero angle. Therefore, the axial velocity field of gate rudder can be imaged whilst the exact position is slightly different because the center of the rotation of the blades is not coincident with the center line of the vessel.

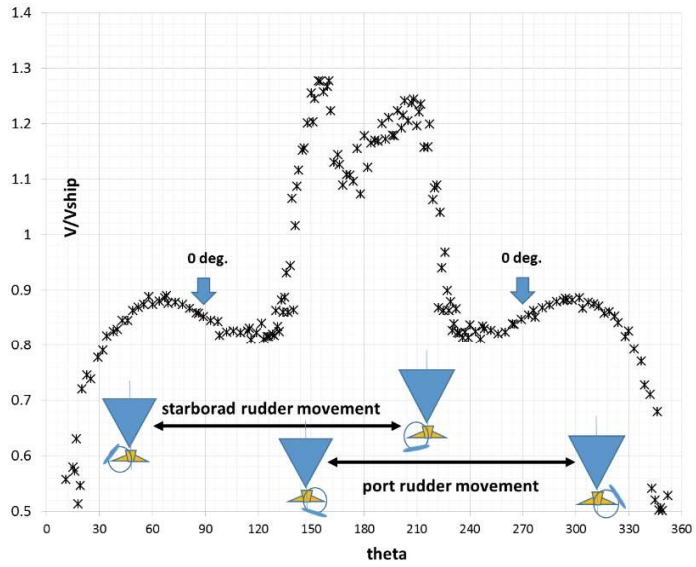

Fig.9 Induced Velocity by a Propeller on a Gate Rudder Moving Plane $(\beta = 0)$

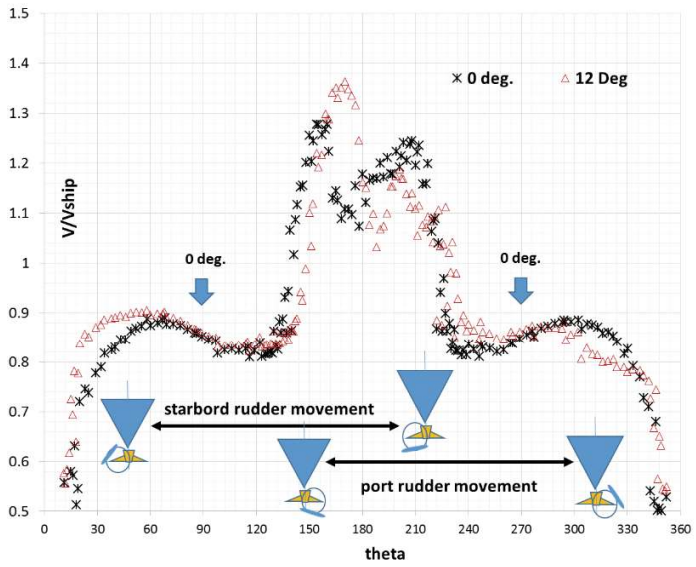

Fig.10 Induced Velocity by a Propeller on a Gate Rudder Moving Plane $(\beta = 0° \& 12°)$

Numerically calculated velocities (U and V) around the GRs position, shown in Fig.9 and Fig.10, were averaged along the virtual span of the GR for the range of effective inflow angle to rudder at each drift angle (β) for 0° and 12°. The gate rudders operating angles are port side blade $50^{\circ} \leq \vartheta \leq 130^{\circ}$ and starboard side blade $230^{\circ} \leq \vartheta \leq 310^{\circ}$. It is already known that the rudder force of Gate Rudder is relatively weak between rudder angles 0° to 35°. However, the rudder force of the Gate Rudder is larger than conventional rudder from 0° to -30° (forward) and over 45° (afterward).
Having a large operating angles is a very good advantage of gate rudder because most of the domestic vessel require larger side force at the port or quay for quicker and safer operations. Sometimes the reputation of high lift rudder such as flap rudder and fish tail rudder is too sensitive during the normal navigation period. The reason is that a rudder specification such as rudder area and wing sections should satisfy the maneuvering performance at the port instead of her navigation period. Fig.10 shows the effect of yaw angle (0° vs. 12°) on the ratio of propeller axial velocity to ship speed. A difference appears near the ship center ($0^{\circ} < \vartheta < 50^{\circ}$ and $150^{\circ} < \vartheta < 180^{\circ}$) remarkably. However, the difference at other rudder position is small.
Fig.11 shows the flow diagram showing how the maneuvering motion estimation using the rudder forces which are calculated based on combination of CFD and aforementioned theories. Fig. 11 is further explained in the section 3.

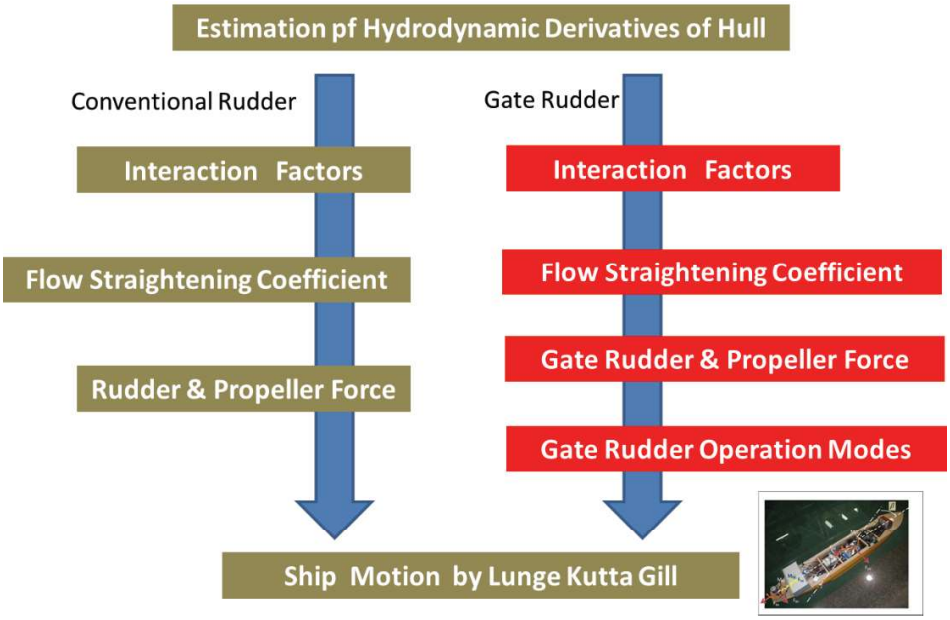

Fig.11 Manoeuvring Simulation of a Ship with Gate Rudder

2.5. Interaction model between a propeller and gate rudder

In order to achieve the main objective of this paper we have to demonstrate how accurate and in a practical way we can predict the interaction between the propeller and gate rudder blades by using the dedicated software tools developed and validated with the results of specific model test data.
For the above purpose we used our dedicated computer program which was developed based on the earlier mentioned the linearized Vortex Lattice Method for the rudder blade and simple lifting surface based propeller theory. The advantage of the VLM is its simplicity and intuitiveness compared to the CFD tools. Addition to this, the flow field surrounding the gate rudder is governed by flow with lesser viscosity because the rudder is almost situated at the outside of thick boundary layer in the stern.

The interaction between the rudder blades of a gate rudder and its propeller can be represented by following phenomena.

(1) Gate rudder is working in a weak non-uniform flow and accelerates the flow in a space between the two rudder blades when the propeller is rotating
(2) Its propeller is working in a thick boundary layer caused by the two rudder blades as such by sucking the flow upstream and ejecting in downstream.

The modelling of the interaction phenomenon based on the above flow physics can be done iteratively and step by step as shown in Figure 13.
The first step is to input a ship wake on the surface of the propeller and rudder blades of the gate rudder. Next step is to obtain the initial performance without interaction for both the propeller and the gate rudder. After this we can start the iterative calculations using the induced velocities calculated by each model. The system is very effective and accurate within the small rudder angle (less than 10deg.), however the rudder force and propeller performance will be not calculated accurately if the rudder blades was exposed to the propeller slip stream. In this region, the system is switched off and changed so as to use another logic such as MMG model etc. which are used for a prediction of ship propulsion and manoeuvring motion[10][11][12]. An available MMG model suite was modified to cater for the gate rudder that will be explained separately in this paper.

From the iterative calculations, the following conclusions are derived.

(3) Gate rudder will guide the larger area of favourable stern flow into the propeller's plane acting as a propeller with larger diameter.
(4) Gate rudder blades generate additional thrust instead of rudder resistance only because of the forward lift generated by the rudder blades .
(5) Propeller of a gate rudder is working in an accelerated flow induced by the rudder blades and the difference of flow fields can be divided into two components: one is accelerated flow due to rudder; and other is no appearance of the rudder displacement effect which can be seen in the conventional rudder case
(6) Propeller of a gate rudder generates contracted flow which increases the angle of attack of the rudder blades.

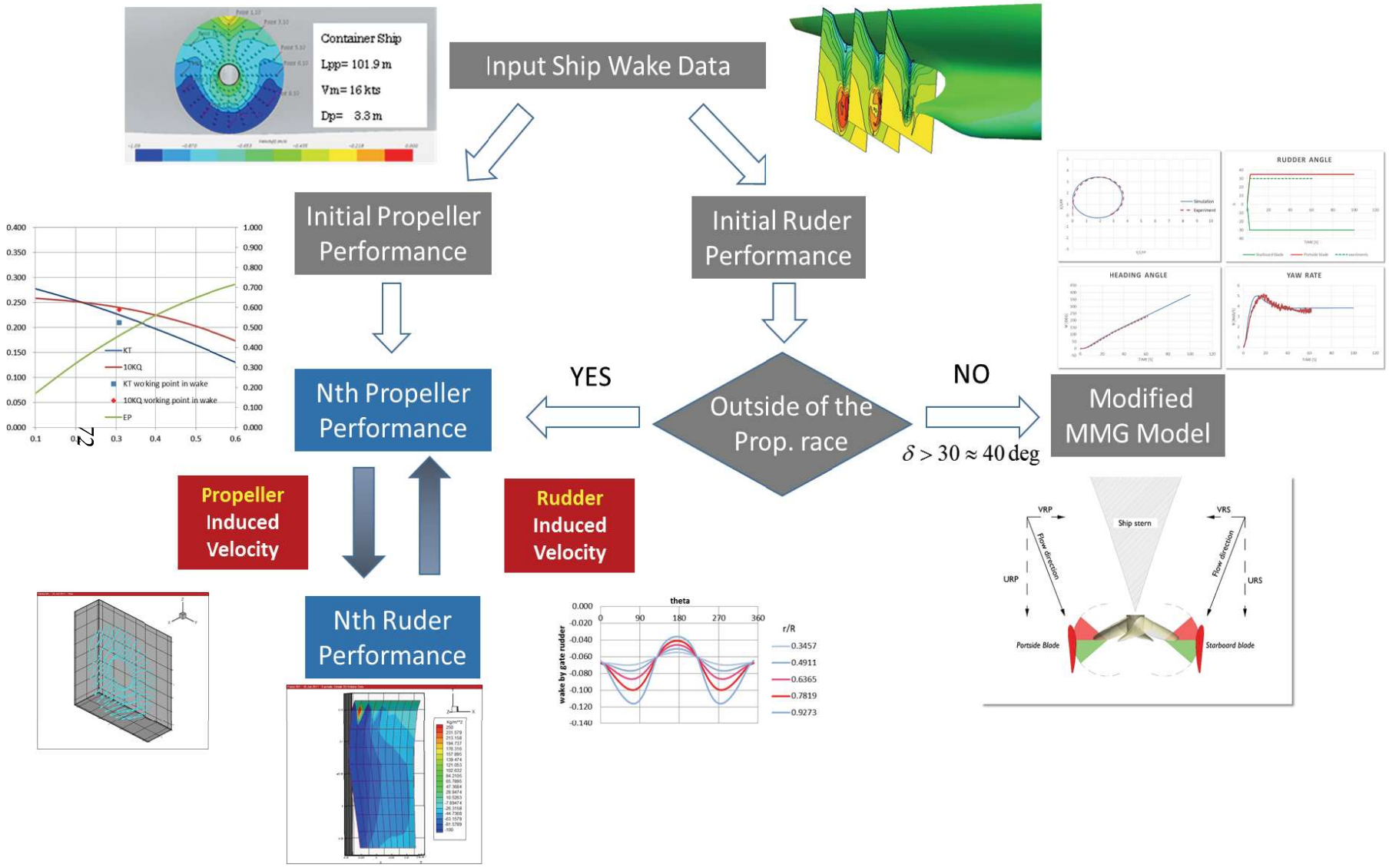

Fig.13 Iterative computation procedure

3. Validation of theories by model tests

As described in the previous sections, we have a possibility of several theories which can be used for design and analysis of gate rudder. For this purpose, it is clear that the most efficient tool should be selected because each theory has its own advantages and disadvantages. For example, the blade element theory can explain the model test results very quickly by introducing the empirical coefficients such as wing profile drag coefficients etc.. However, this theory cannot be used for the prediction of flow fields and also requires accurate information of flow vectors on the wing surfaces. Addition to this, there are no information about lift/drag distributions on the blade surface which affect the moment characteristics the blade or rudder.

In Table 1, we can see the important model tests which were conducted during various gate rudder projects. The details of some of these model tests and comparison of the data with the theories described in the previous section will be introduced in this section.

Table 1 - List of Model test related to Gate Rudder

	ship type	model size	facilty	resistance & Propulsion test	rudder force measurement	ship motion	wake measure.	flow measure.	flow visualization
case 1	bulk carrier	6	NMRI	X	X				
Case 2	domestic cargo	2	FEL	X	X				X
case 3	bulk carrier	6	NMRI	X	X				
case 4	domestic cargo	2	FEL	X	X		X	X	X
case 5	domestic cargo	2	FEL	X					X
case 6	open water		ECT	X	X			X	
case 7	dummy ship	2.5	ECT	X	X				
case 8	domestic cargo	2	FEL	X	X				X
case 9	domestic cargo	2.5	KU	X	X	X			
case 10	domestic container	2	FEL	X	X				X

3.1 Panamax Bulk Carrier Model with standard beam (Case1)

The twin rudders behind a propeller called “Frame Rudder” (Initial version of gate rudder was investigated not only by model scale tests but also by full-scale tests (full scale data cannot be disclosed here due to the contract) as shown in Figure 17. The advantages of this rudder is its small chord length compared with the original single rudder. The chord length of the Frame Rudder can be reduced by almost half because the rudder has two blades behind the propeller with an adequate distance. This will make it possible to reduce the noise and vibration of the vessel. This fact was confirmed very clearly by the full scale ship during the sea trial. It seems that there are two reasons for this advantage. One possible reason is the small flow disturbance from the rudders on the propeller plane. As we know well, the conventional single rudder induces displacement wake on the propeller centre plane and the mean value of this wake is around 4% according to ITTC powering procedure. However, it is obvious that the wake is not distributed on the propeller plane uniformly. The wake must be condensed in the centre line of the vessel where the higher ship wake can be seen.

The wake of the rudder increases the wake peak on the centre line and this in turn increases the noise and vibration.
Next reason of favourable noise and vibration may be reduction of the vibration of the rudder itself which may be introduced by the strong vorticities from the propeller. The most powerful vortex is a hub vortex originated from the propeller hub and it may hit the rudder blade if the rudder is located in the centre of

the ship. Another fact, which was obtained from the sea trial of the full-scale vessel, is small difference in the speed performance. There was no remarkable improvement in the vessel performance.

Three components of the rudder force were measured for a conventional (high lift type) and the Frame Rudder at 400m towing tank of NMRI (National Maritime Research Institute) as shown in Fig.14.

Fig.14 - Twin rudder installed on the 6m long model

Table 2 - Rudder force measurements of three types of rudders

Rudder	Conventional	High lift rudder	Twin rudder A	Twin rudder D
α	1/11.164			1/12.341
Height(m]	0.26	0.26	0.26	0.2269
Chord[m]	0.1252	0.1252	0.055	0.0689
λ	2.0767	2.0767	4.4545	3.2932
Area [m2]	0.0326	0.0326	0.027	0.0313
Ld/Ar	67.9	67.9	82.0	77.3
Distance of rudder	-	-	0.138	0.1036

The blade element theory and the momentum theory were used for the predictions of the force on the rudders and comparisons with the experiments. The rudder normal forces are predicted by the following equations which are derived from Equation (3) as explained in Section 2.1.

$$
\begin{aligned}
&F_N' = \frac{F_N}{0.5\rho V_R^{\,2} \cdot A_R} \\
&F_N = F_{N1} + F_{N2} + F_{N3} + F_{N4} \\
&F_{N1} = 0.5 \cdot C_L \cdot \rho V_{R1}^{\,2} A_{R1} \quad V_{R1} = V_S * (1 - w_1) \\
&F_{N2} = 0.5 \cdot C_L \cdot \rho V_{R2}^{\,2} A_{R2} \quad V_{R2} = V_S * (1 - w_2) \cdot \varepsilon \cdot \sqrt{1 + C_T} \\
&F_{N3} = 0.5 \cdot C_L \cdot \rho V_{R3}^{\,2} A_{R3} \quad V_{R3} = V_S \cdot (1 - w_3) \\
&F_{N4} = 0.5 \cdot C_L \cdot \rho V_{R4}^{\,2} A_{R4} \quad V_{R4} = V_S \cdot (1 - w_4) \\
&C_L = 2\pi\delta \frac{2\lambda}{2.3 + \lambda}
\end{aligned}
\tag{17}
$$

where, F_N is rudder force (kgf) which is measured in normal direction acting on rudder blades. V_R is velocity at rudder position and V_S denotes ship speed and w_1 to w_4 represent wake at each rudder position as shown in Figure 15.

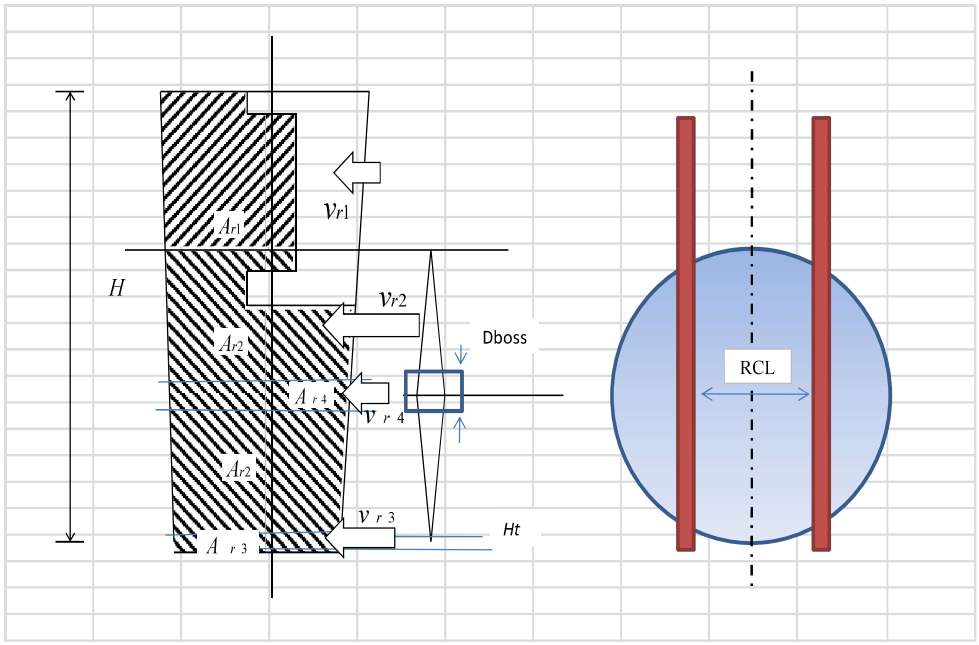

Fig.15 - Co-ordinate system of Rudders & Propeller

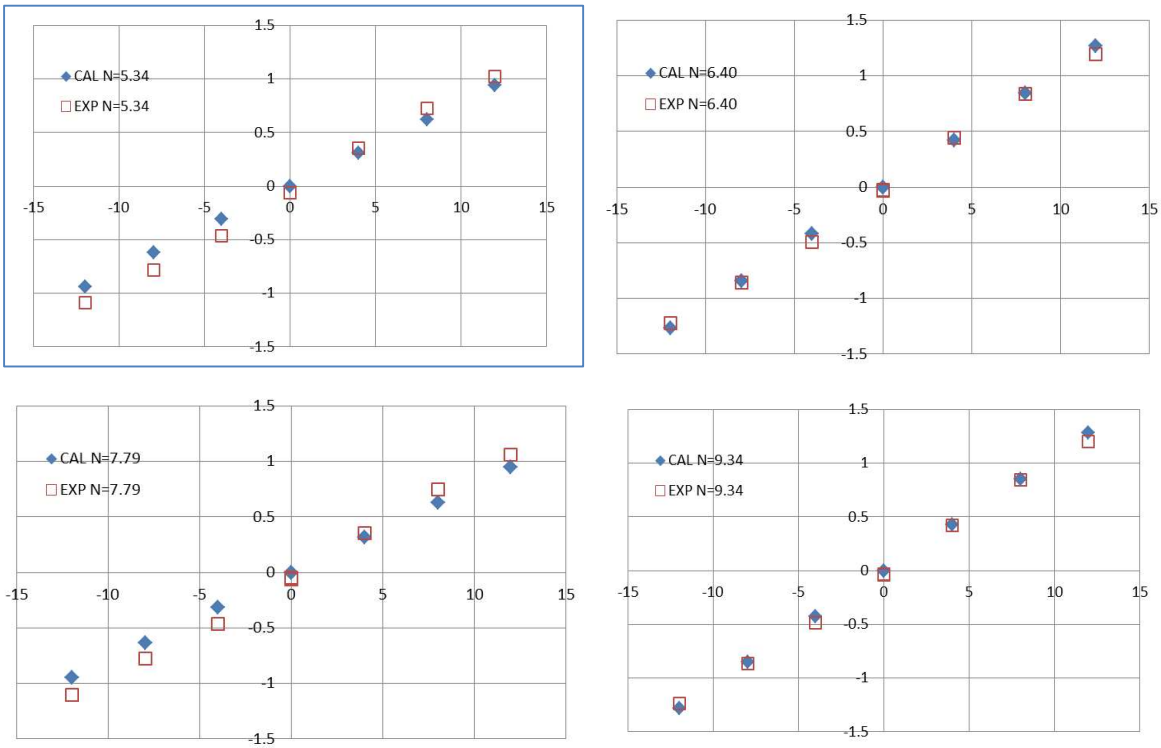

Fig.16 - Rudder normal force of twin rudders behind a Propeller

Fig.17 - Installation of Frame Rudder on domestic cargo ship (March 2011)

As shown in the Figure 16, the rudder normal forces behind the propeller can be predicted with the reasonable accuracy even if the rudder is not located in the ship centre. However, there is an important parameter in this prediction which is the empirical factor of ε. As explained in Equation (17), ε is a function of x/D_p and r/R. In the above predictions, constant ε=0.85 was applied by taking the computation results from the simple propeller theory as explained in the previous section.

This experimental data is invaluable from the aspect of verification of a program which we are using for the prediction of the propeller slip stream. It is also important to note that the rudder force can be summed by two forces originated from different parts of the rudder, one of which is the rudder force outside of the propeller slip stream while the other one is the rudder force inside of the propeller slip stream which is more important than the former one.

3.2 Bulk Carrier Model with wide beam (Case 3)

Among the model tests dedicated to the investigation of the gate rudder performance, this model is the biggest one (see Table 3) and the measured values are expected to be more accurate thanks to the high Reynolds number which may give accurate lift and drag acting on the rudder.

Figure18 (left) shows the after body of the vessel in full scale. The rudder forces are predicted by giving information about the inflow at the rudder position. The rudder section and the direction of the nose-tail line are the most important design parameters. Before making the gate rudder model, we should pay attention to the flow field surrounding the rudder. In this project, the flow field was calculated by CFD (Neptune) [9] and investigated the flow direction against each section of the gate rudder. These information can be seen Figure18 (right) which shows the normalized flow velocity and flow angle

distributions. From these information, it was predicted that the rudder thrust will show the peak point around 11m water line.

The measured rudder forces and moments are shown in Figure 19 where we can see the differences in the two prediction methods. BET and VLM represents the blade element theory and vortex lattice method, respectively. Moment N (Nm) of BET was calculated by assuming the position of centre of effort as 32% cord from the leading edge.

Table 3 - Principal dimensions and photo

	Full Scale	Model
Lpp (m)	300	6.0
B (m)	65.0	1.2
draft (m)	17.9	0.358
CB	0.80	
Prop. Dia.(m)	8.50	0.170
Rudder Area (m**2)	59.5*2	0.0238*2

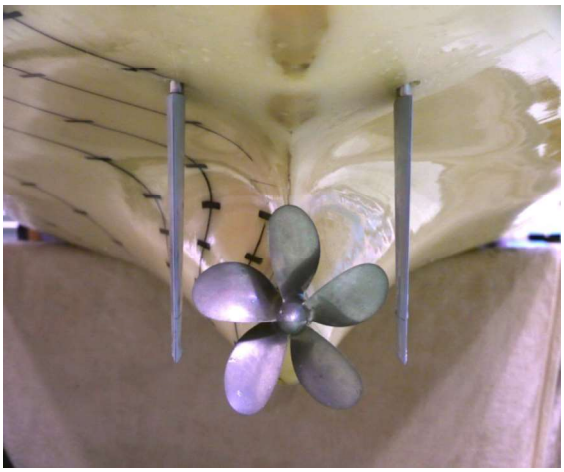

As shown in these figures, the agreement between the theories and experiment is acceptable except for the Fx prediction based on VLM. The reason of this discrepancy is not clear, however we have to bear in mind that the input velocity data was not measured which may include some error.
.

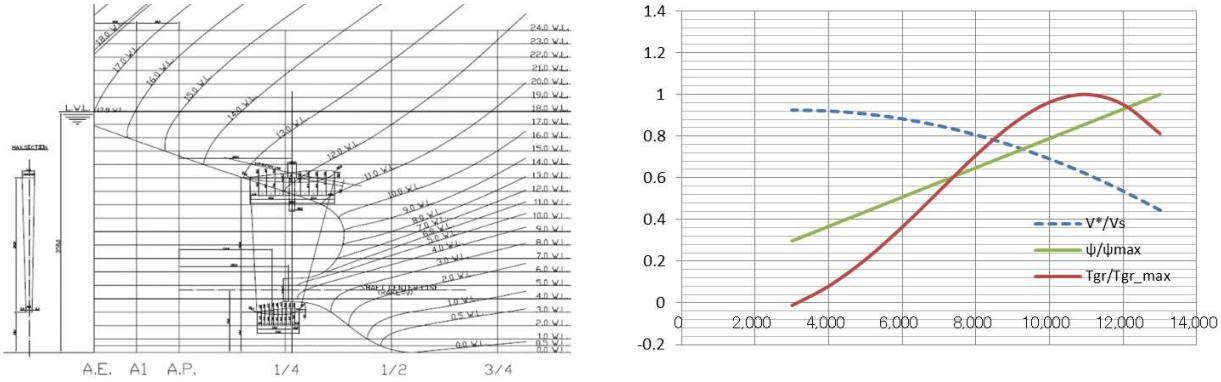

Fig.18 - After body and inflow data of Bulk Carrier Model

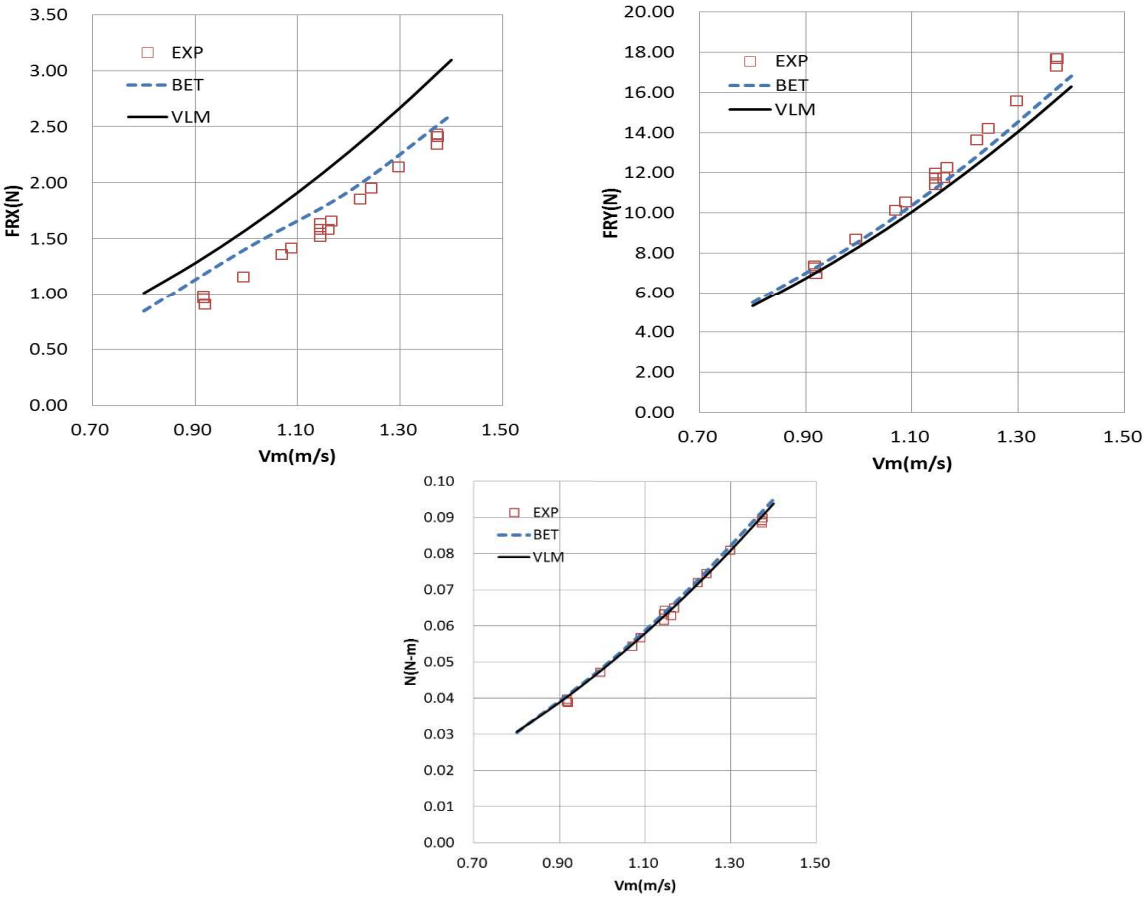

Fig.19 - Comparison of F_{RX} , F_{RY} and N_{RZ} between theories and experiments.

3.3. Detailed measurement of forces and flow field of gate rudder at ECT (Case 6)

The validation of the output data of computational tools by the model tests is very important for the accurate modelling the propeller and rudder interaction and reliable computational tools can be very useful and effective, as the model tests can be time consuming, expensive and sometimes difficult to conduct.

Table 4 Dimensions of CPP model

Dimensions	unit	Model Scale
Diameter	m	0.2639
Pitch Ratio at .7R	-	0.60
Expanded Area Ratio	-	0.47
Boss Ratio		0.253
Number of blades	-	4

Model tests in the Emerson Cavitation Tunnel (ECT) of Newcastle University were carried out as a part of the present research in order to measure the velocity field around the rudders and the propeller accurately. Figure 20 shows a side view of ECT and the set up of measurements.

The gate rudder model was designed for the domestic cargo as mentioned in Table 1.

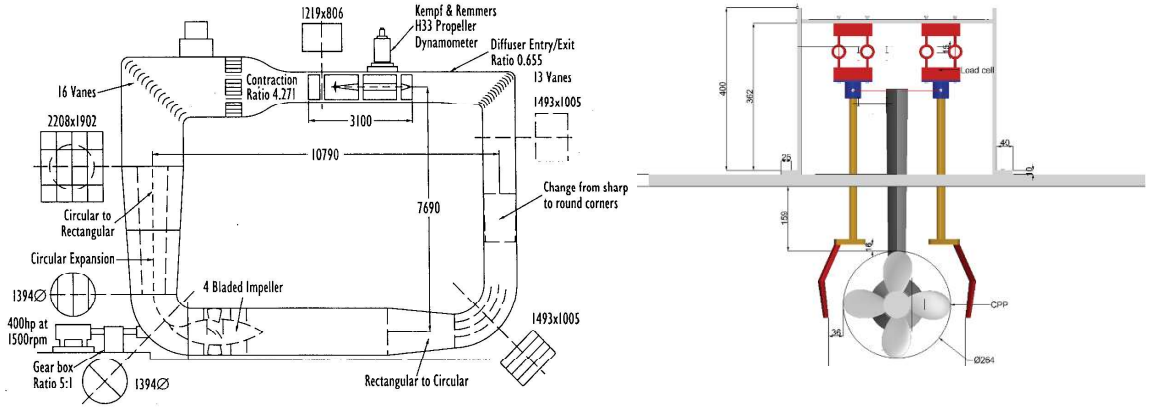

Fig.20 - Emerson Cavitation Tunnel (left) and Gate rudder set up (right)

The scale of the gate rudder model was decided to match the model propeller with a diameter of 0.2639m as shown in Table 4.

The flow velocity measurements were conducted by a combined Laser Doppler Anemometry and Phase Doppler Anemometry (LDA/PDA) system of Dantec Measurements Technology and associated data collected by the LAB view software environment which also provides online data analysis capability. See Fig. 23 for the LDA set up.

Experiments were carried out by using a controllable pitch (CP) model propeller, shown in Fig. 21, which was manufactured by Kamome Propeller Co., Ltd. The general characteristics of the model propeller are given in Table 4. This 4-bladed model propeller is equipped with a hub upon which each of the four blades is mounted with a bolt. Blade angle adjustment is possible by loosening the bolts with a screw and turning the blade into the desired blade angle with the help of an adjusting tool provided together with the propeller as shown in Fig. 21. The digital measuring device presented in Fig. 21 is equipped with a gauge which is set to measure the height difference between the hub and a reference point upon the blade. The measured value is used to read from a table provided by the manufacturer and the corresponding blade angle value assigned to it.

The measurements were intended to conduct with the gate rudder model and the propeller model in the uniform flow of ECT. In order to eliminate the uncertainty of the inflow to the system, non-uniformity of the flow field of the test section was investigated and the result is shown in Fig. 22-Fig.24.

Fig.21- Pitch setting of CPP model

Table 5 – Test matrix for flow field measurements

CPP (B.A)	Rudder	Vm (m/s)	n (rps)	Flow Meas.	T (N)	Q (N-m)	Vx at GR	Vy
15.26	without rudder	0.9	9.31		57.95	1.757	-	-
	without rudder	0.33	6		32.6	0.881	-	-
	G.R. (0deg.)	0.9	9.31	6 sections	57.95	1.757	0.9	0.183
	G.R. (0deg.)	0.33	6	6 sections	32.6	0.881	0.33	0.134
15.26	G.R. (10deg.)	0.9	9.31	6 sections	57.95	1.757	0.9	0.183
	G.R (20deg.)	0.9	9.31	6 sections	57.95	1.757	0.9	0.183
8.26	G.R. (0deg.)	0.33	9.31	6 sections	28.094	0.722	0.33	0.157
	G.R. (10deg.)	0.33	9.31	6 sections	28.094	0.722	0.33	0.157
	G.R. (20deg.)	0.33	9.31	6 sections	28.094	0.722	0.33	0.157
0.26	G.R. (0deg.)	0.33	9.31	6 sections	5.3	0.376	0.33	0.047
	G.R. (10deg.)	0.33	9.31	6 sections	5.3	0.376	0.33	0.047
	G.R. (20deg.)	0.33	9.31	6 sections	5.3	0.376	0.33	0.047

conducted at Emerson Cavitation Tunnel

Table 5 shows the selected conditions for the tests. The pitch angles for the CP propeller was set at 15.26 deg., 8.26 deg. and 0.26 deg.

During the tests, not only propeller and rudder forces but also flow fields around the propeller and the rudder were measured at 6 sections of axial direction as shown in Figure 22.

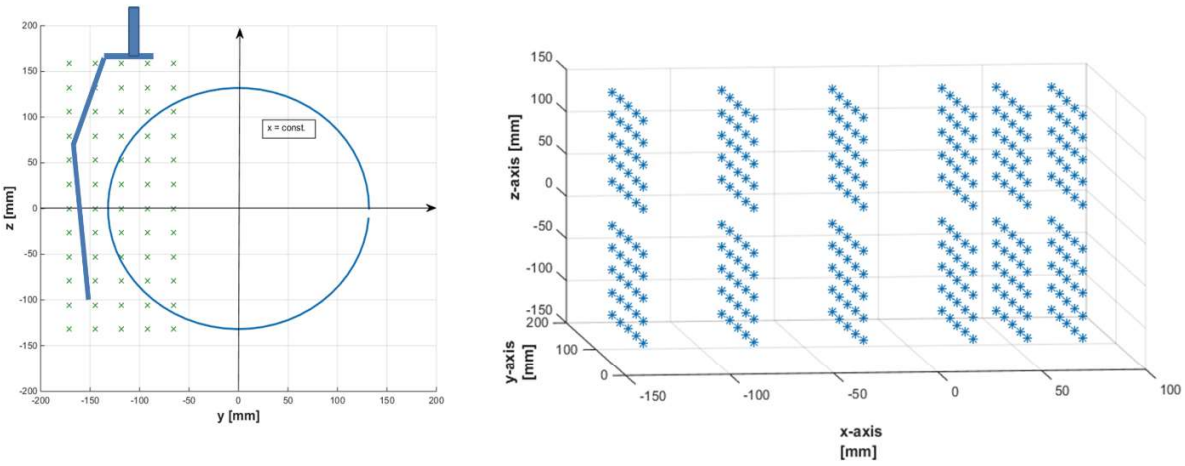

Fig.22 - Measurement points by LDA (left: y-z plane, right: bird eye view)

The results of the LDA measurements are shown in Figure 24 and 25 while the results of the predictions are shown in Fg.26. The comparison of the flow measurements with the calculations are displayed in Figure 26 whereas the comparison of the measured forces and moments with the computational predictions are shown in Figure 28.

According to the LDA measurements, the flow field around the gate rudder model were captured accurately except the near points of the gate rudder surface where the flow may not be stable and the data rate of the LDA is not enough for measurement. This tendency also can be seen near the propeller tip as shown in Fig.27. This figure shows the comparison of the flow field specifically at (x = 0.1D ; y = 0.0D) which is the location just after the propeller and at the same level with the propeller shaft.

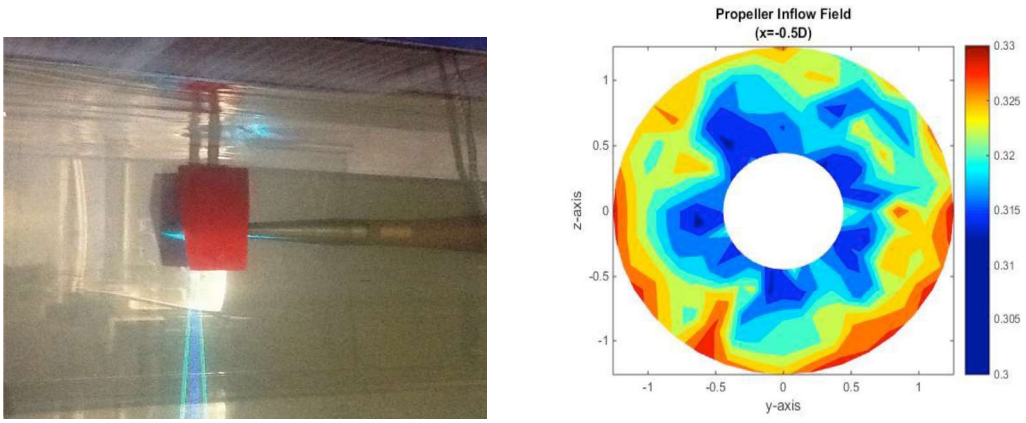

Fig.23 - LDA measurement set-up (left) and measured flow field at propeller plane

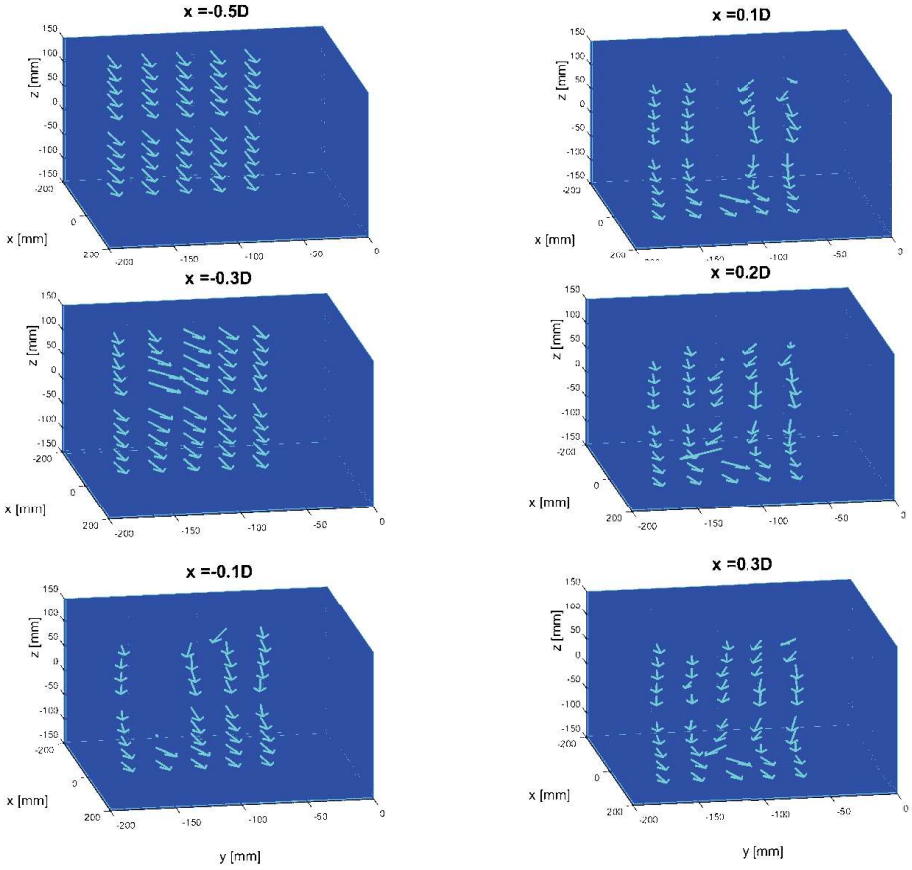

Fig.24 - Results of LDA measurements around gate rudder at $\delta = 0.0\,\mathrm{deg}$

Fig.24 shows the LDA measurement results in case of $\delta = 0\,\mathrm{deg}$. around the gate rudder. Data presented at x= -0.5D and x= -0.3D are the measured values at upstream i.e. before the flow is getting into the two rudder blades and data presented at x=0.2D are the measured flow field at the downstream of the gate rudder. Data presented at x= -0.1D and x= 0.1 D are the measured flow flow field inside the gate rudder (i.e, between the two rudder blades). The effect of the rudder blades can be seen in the vicinity of the leading edge of the gate rudder at x=0.3D. The flow is twisted by the rudder blades and sucked by the propeller. This appears to be the clear evidence of a strong leading edge suction on the rudder blades and hence producing the rudder thrust as the most important benefit of the gate rudder system.

As shown in Figure 24 there are points where the data could not be obtained at x= -0.1D and x= 0.1D. These points were too close to the rudder where the data rate were quite low. After the position at x=0.1D, the flow can be characterized by the swirling action of the propeller flow.

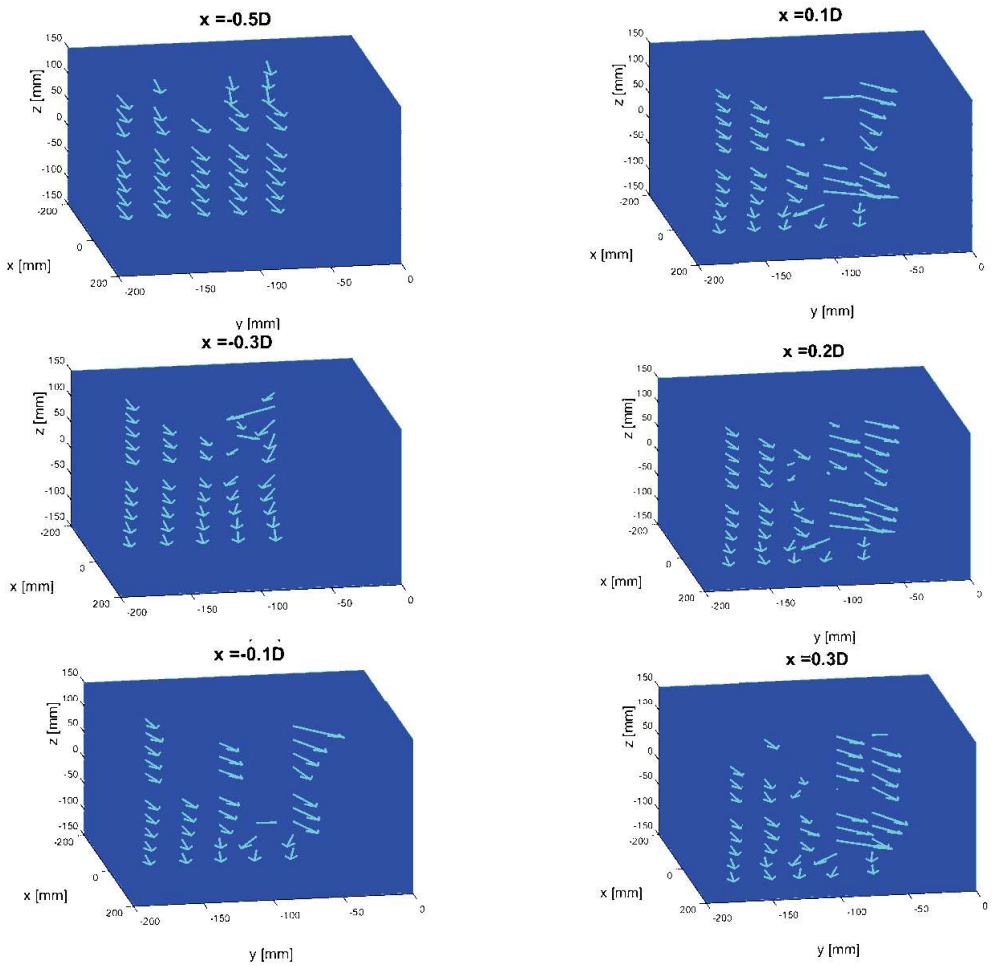

Fig.25 - Results of LDA measurements around gate rudder at $\delta = 20.0\,\mathrm{deg}$

Figure 25 shows the flow field around the gate rudder at 20 deg helm angle. The difference in flow filed compared to the field presented in Figure 24 appears to be at further upper stream. The first distinguished flow can be seen on the centre line of x= -0.3D. From the position at x=-0.1D, the flow is largely shifted by the rudder and the main flow is diverted to starboard side except outside region of the gate rudder. At the downstream of the gate rudder, the swirling action of the propeller is not so clear.

The induced velocity due to rudder and propeller was calculated in the uniform flow conditions under the same propeller /rudder geometry and the same propeller loading conditions. The results are shown in Figure 26. The left of Figure 26 presents the rudder induced velocities on the propeller plane in transverse direction, z(m) position. From this figure it is clear that the total axial velocity is increased as a result of the increased induced velocities in the vicinity of the rudder blades (where uu is due to the starboard rudder blade and + uu` is due to the port side rudder blade) The mean value of the induced axial velocity is around 0.05m/sec while the propeller advance speed is 0.9m/sec. This means the propeller advance speed is accelerated by the gate rudder by 5.5% which is close to the values obtained from thrust identity method. Figure 26 (right) shows the superposed induced velocity of the rudder blades and the propeller. This can be used for the rudder performance again as shown in Fig.13.

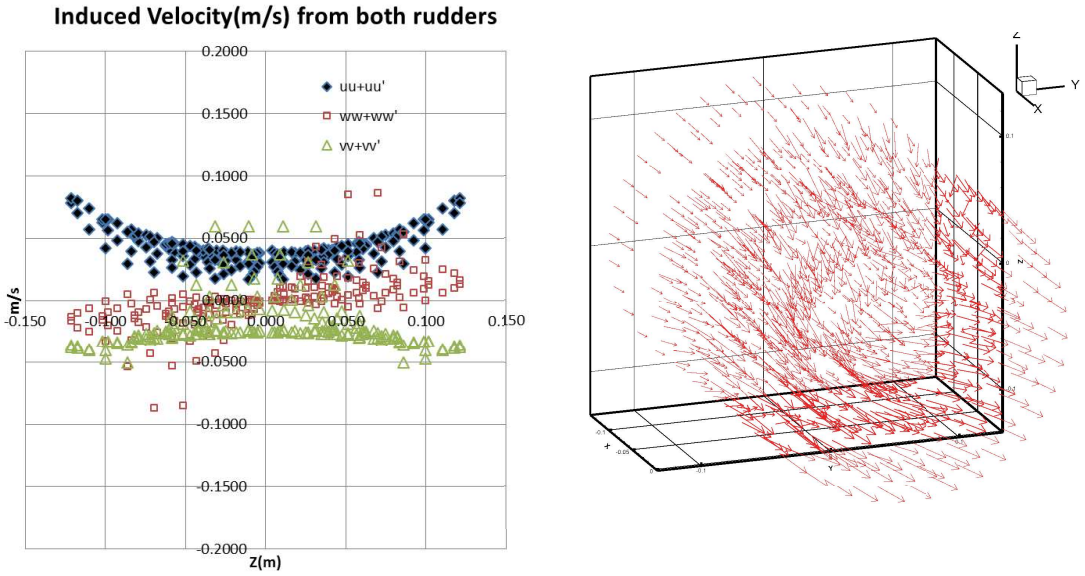

Fig.26 - Obtained results from Interaction Model

Figure 27 shows the comparison of the numerical predcitions and experimental measurements taken at position of x= 0.1 D and y = 0.0 D which is corresponds to a distance of 10% downstream of the propeller and at the shaft centre level. As it can be seen in Figure 27 the computations were conducted at the outer edge of the propeller slip stream, z= 0.125 while the propeller radius is at z= 0.132. The measured values at z= 0.120 are scattered reflecting the instability of the tip vortex shedding from the propeller. As shown in this figure despite the predicted axial velocities are slightly high, the velocity distribution and the outer edge of the propeller slip stream are well predicted.

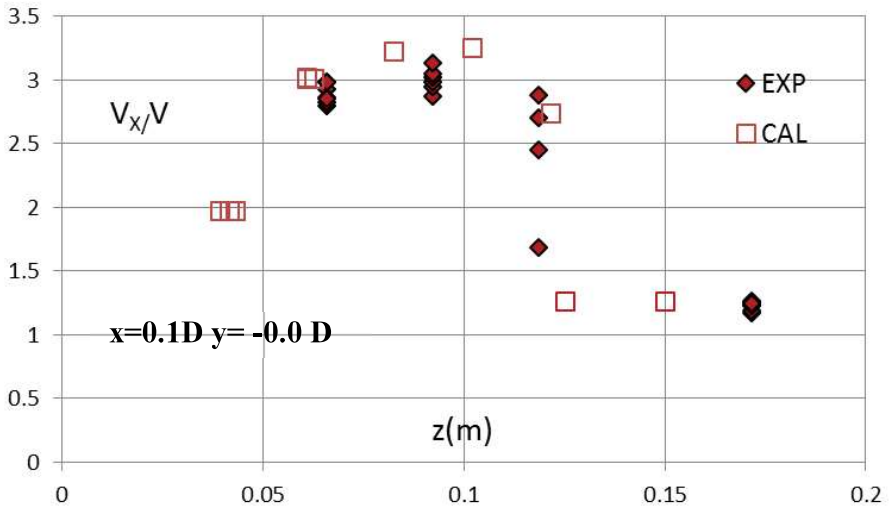

Fig.27 - Comparison of axial velocities between experiments and calculations

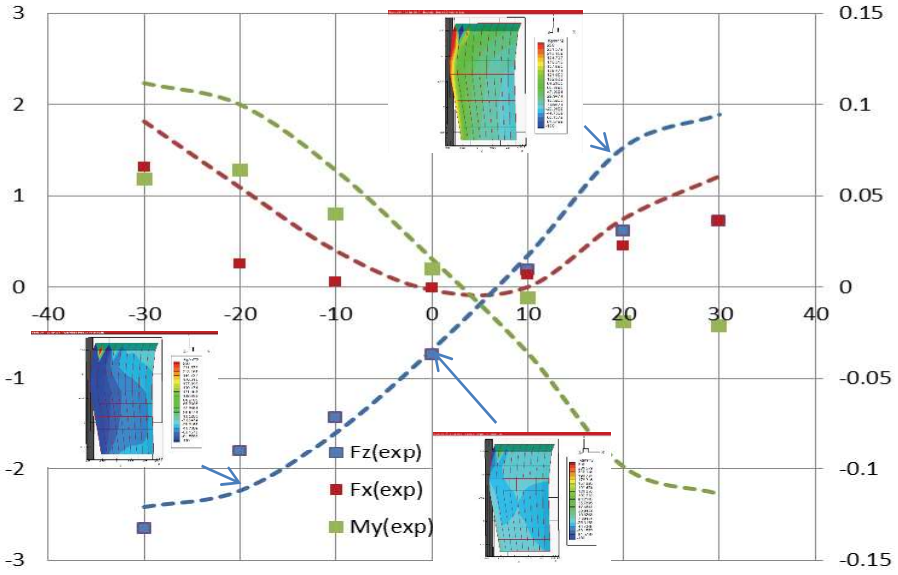

Fig.28 - Comparison of rudder forces between experiments and calculations

Finally, Figure 28 shows the comparison of the rudder forces between the experiments and the calculations. In this comparison, we should bear in mind the limitations of the applicability range of the linearized vortex lattice method in terms of the rudder angle. It may be assumed that the applicable range for the rudder helm angle is between -10deg. to +10deg. Based on this assumption and Figure 28, the following comments can be made for the general tendency of the differences observed:

(1) For rudder angles over 10 deg., the experimental rudder normal force Fy is rather small compared to the calculated force and this may be related to the effect of the flow separation for rudder angle over 10 deg. (Note that model test based Rn =$1.1*10^5$)
(2) The difference in moments My between the calculations and experiments is brought by the difference in the measured rudder normal force Fy which is smaller than the predicted values.

4. Conclusions

This paper presents further developments on A new concept rudder system which is called "Gate Rudder" and presented a recently developed dedicated design analysis and simulation software to predict the manoeuvring performance of a gate rudder system. The software has been developed as a practical design tool by which one can analyse and simulate the manoeuvring performance of a ship equipped with a gate rudder system accurately by taking into account the interaction between the asymmetric rudder blades and the propeller.

In the paper five different numerical prediction methods have been evaluated by using the model test data on three different ship types equipped with various versions of the gate rudder systems.

While the evaluation of the prediction methods indicated that each method has its own advantages and disadvantages, amongst the five methods evaluated, the simple propeller theory combined with the linearized vortex lattice theory appeared to be the most effective method providing basis for a practical design and analysis software.

In addition, the CFD can be very useful supporting design and analysis tool at the last stage of the gate rudder design/analysis where the hull stern shape, propeller and gate rudder geometry including a detail of the position are already designed using other numerical tools.

The blade element theory is useful for predictions at large angle of attack because the separation and drag coefficients can be easily implemented in the theory based on the empirical data. This is the reason why this theory is often used for manoeuvring simulation (e.g. in modified MMG theory).

5. Acknowledgements

We would like to express our sincere gratitude to Dr. Weichao Shi (Strathclyde University) and PGS Alessandro Carchen (Newcastle University) for their support through the CFD calculations and modified MMG program development.

Additionally, we would like to thank Messrs. H. Yanaizumi, M. Yazawa and T. Imai of Kamome Propeller Co. Ltd. for all their help throughout the model tests preparation and program development of vortex lattice method.

Finally, we would like to express our thanks to Messrs. T. Matsuzaka (K-7 Co. Ltd.), T. Takeda (Yamanaka shipbuilding Co. Ltd.) and T. Kurokawa (Yamanaka shipbuilding Co. Ltd.) for their support to the design of full scale gate rudder which will be installed on the newly build container ship and delivered by the end of November 2017.

This work was supported by the foundation of Japan Ship Machinery and Equipment Association.

6. References

1-5. Kuribayashi K. "The new hull form with twin rudders utilizing duct effects (1^{st}-5^{th} report)" Proceedings of Conference of JASNAOE, 2015-2017

6. Turkmen S., Sasaki N., Atlar, M., Miles, A., Takeda, T. "The gate rudder application to improve ship's poor course keeping ability" A.Y. Odabasi Colloquium, November 2016,

7. Yamasaki R. "On the propulsion theory of ships on still water − Introduction−" Memories of the Faculty of Engineering, Kyushu University, Vol. 27, 1968

8. Nakatake K., "Application method to calculate propulsive performance of ships", Memories of the Faculty of Engineering Kyushu University vol.41, 1981

9. Hino, T. et al., Proc. of 8th International Conference on Numerical Ship Hydrodynamics, 2003.

10. Yasukawa A. and Yoshimura Y. " Introduction of MMG standard method for ship manoeuvring predictions" JMST, Volume 20, Issue 1, pp37-52, March 2015

11. Carlton J. "Marine propellers and propulsion" 13.3. Rudder-Bulb Fins System, Butterworth-Heinemann, P341, 2012

12. Molland AF. and Turnock SR, "Marine rudders and control surfaces, Boston p15, 2007

13. Sasaki N. Atlar M. and Kuribayashi S., "Advantage of twin rudder system with asymmetric wing section aside a propeller" JMST July 2015